ISCI, Volume *23*

Supplemental Information

PRMT5 Cooperates with pICln to Function as a Master Epigenetic Activator of DNA Double-Strand Break Repair Genes

Jake L. Owens, Elena Beketova, Sheng Liu, Samantha L. Tinsley, Andrew M. Asberry, Xuehong Deng, Jiaoti Huang, Chenglong Li, Jun Wan, and Chang-Deng Hu

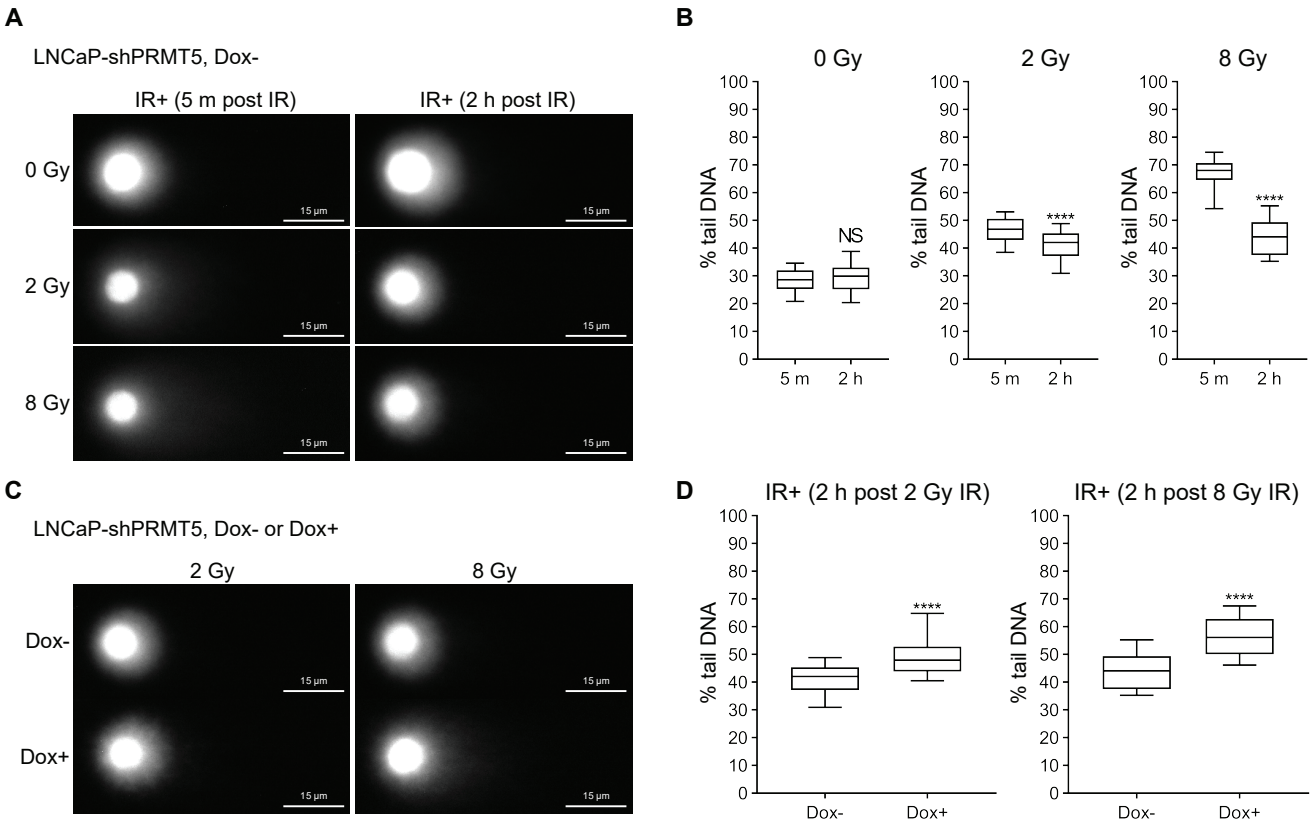

Figure S1. PRMT5 regulates the repair of IR-induced DSBs in prostate cancer cells. Related to Figure 2.

(A) Migration of DNA via neutral comet assay at the indicated time points post the indicated dose of IR in LNCaP- shPRMT5 cells without (Dox-) PRMT5 knockdown. The 5 m time point indicates how much DNA damage is induced by the indicated dose of IR. The 2 h time point indicates how much DNA damage is repaired within 2 h post the indicated dose of IR.
(B) Quantification of DNA damage in each individual cell via calculating the relative amount of DNA in the tail vs. head of the comet ('% tail DNA') from A.
(C) Migration of DNA via neutral comet assay 2 h post indicated dose of IR in LNCaP-shPRMT5 cells with (Dox+) and without (Dox-) PRMT5 knockdown.
(D) Quantification of DNA damage in each individual cell via calculating the relative amount of DNA in the tail vs. head of the comet ('% tail DNA') from C.

Box and whiskers plot in B and D show the median value (line), interquartile range (box), and 10-90 percentile (whiskers) of pooled '% tail DNA' values from 3 independent experiments. Statistical analysis comparing experimental to the control ('Dox-') was performed using Mann-Whitney U-test (**** $P \leq 0.0001$ and NS $P > 0.05$).

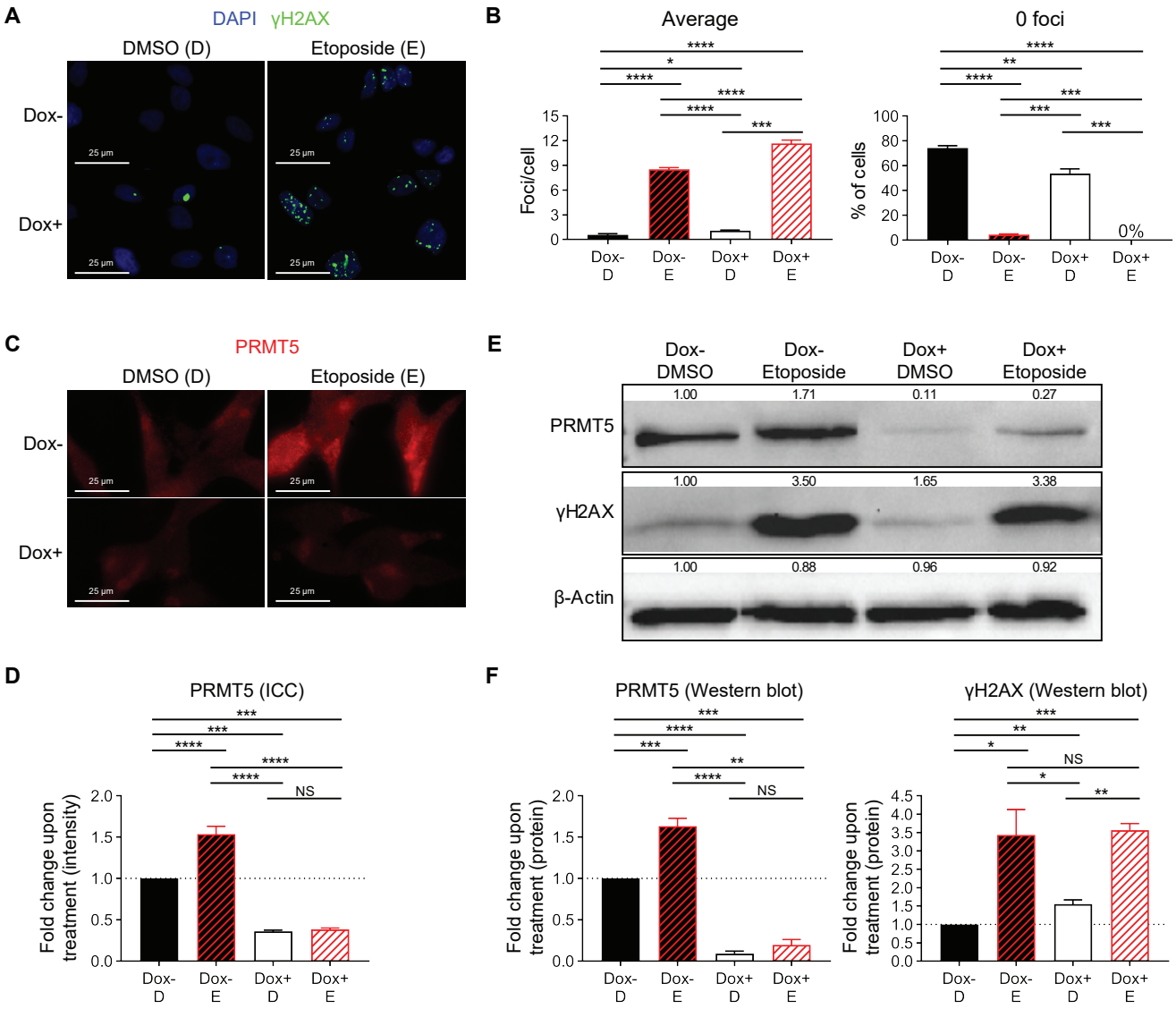

Figure S2. PRMT5 regulates the repair of etoposide-induced DSBs in prostate cancer cells. Related to Figure 2.

(A) DSBs after 48 h of etoposide (E) or DMSO (D) treatment in LNCaP-shPRMT5 cells with (Dox+) and without (Dox-) PRMT5 knockdown.
(B) Quantification of DSBs in each individual cell from A as described in Figure 2B.
(C) PRMT5 expression in cells from A.
(D) Quantification of PRMT5 expression in images from C. For each biological replicate, values were normalized to the value for 'Dox-,DMSO' to calculate the fold change in protein expression upon treatment.
(E) Representative western blot showing changes in protein expression in cells from A. Values shown indicate the intensity relative to 'Dox-,DMSO' for the biological replicate used as the representative western blot.
(F) Quantification of protein expression via western blotting from E. For each biological replicate, values were normalized to the value for 'Dox-,DMSO' to calculate the fold change in protein expression upon treatment.

Fluorescence images in A and C are representative immunocytochemistry images (blue = DAPI, green = γH2AX, and red = PRMT5). Bars in B are the mean ± s.d. of 4 independent experiments and bars in D and F are the mean ± s.d. of 3 independent experiments. Statistical analysis was performed using Brown-Forsythe and Welch ANOVA followed by Dunnett's T3 multiple comparisons test (* $P \leq 0.05$; ** $P \leq 0.01$, *** $P \leq 0.001$, **** $P \leq 0.0001$, NS $P > 0.05$).

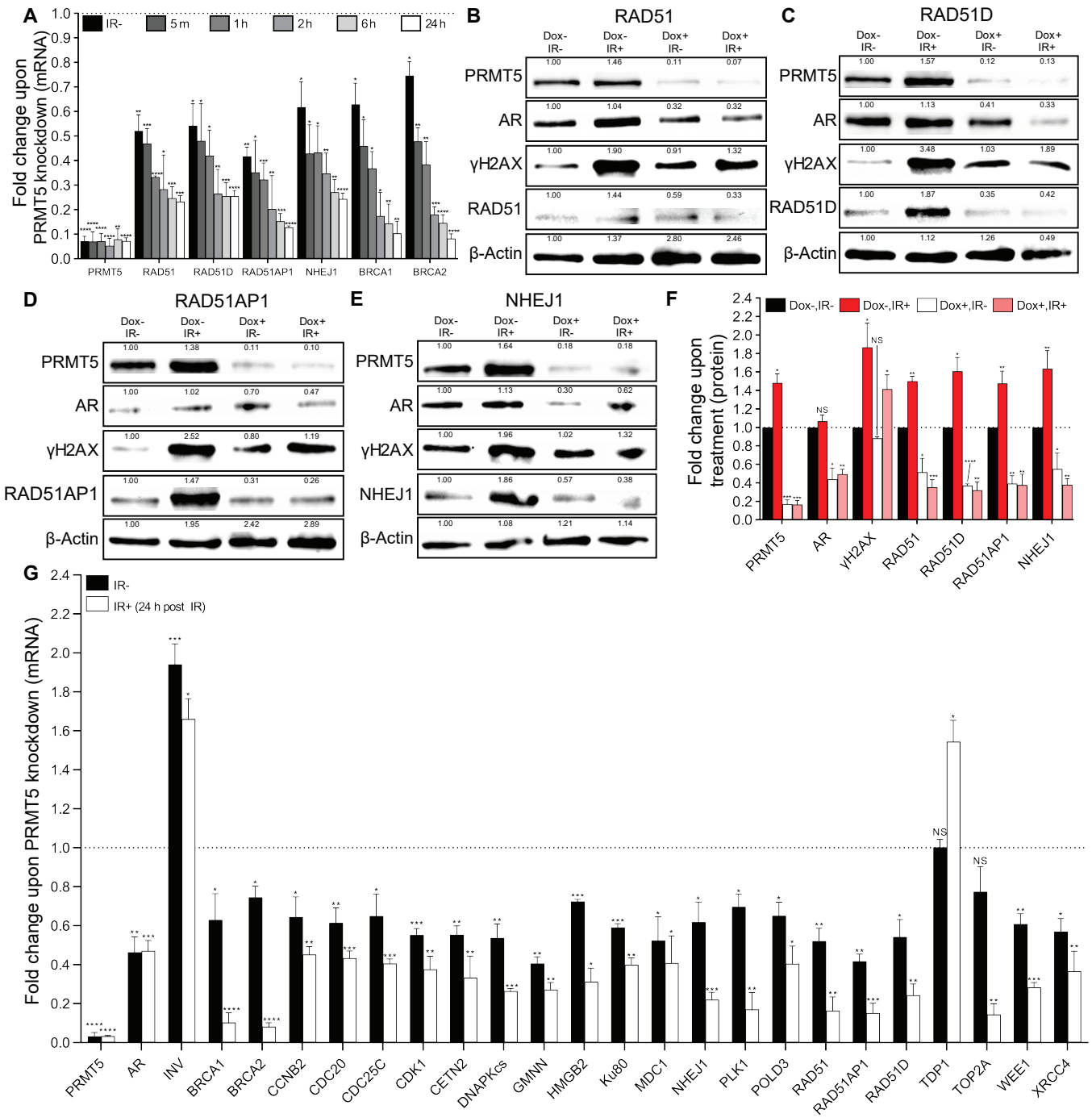

Figure S3. PRMT5 activates transcription of genes that encode proteins involved in the repair of DSBs. Related to Figure 4.

(A) Quantification of mRNA via RT-qPCR at the indicated time point post 2 Gy IR in irradiated (IR+) and non-irradiated (IR-) LNCaP-shPRMT5 cells with (Dox+) and without (Dox-) PRMT5 knockdown. For each biological replicate, the value for Dox+ was normalized to the value for Dox- to calculate the fold change in mRNA expression upon PRMT5 knockdown (See also Figure 4B).

(B)-(E) Representative western blots showing protein expression at 6 h post 2 Gy IR in irradiated (IR+) and non-irradiated (IR-) LNCaP-shPRMT5 cells with (Dox+) and without (Dox-) PRMT5 knockdown. Values shown indicate the intensity relative to IR- for the biological replicate used as the representative western blot.

(F) Quantification of protein expression via western blotting from B-E. For each biological replicate, values were normalized to the value for 'Dox-/IR-' to calculate the fold change in protein expression upon treatment.

(G) Quantification of mRNA via RT-qPCR 24 h post 2 Gy IR in irradiated (IR+) and non-irradiated (IR-) LNCaP- shPRMT5 cells with (Dox+) and without (Dox-) PRMT5 knockdown. For each biological replicate, the value for Dox+ was normalized to the value for Dox- to calculate the fold change in gene expression upon PRMT5 knockdown (See also Figure 4A and 4F).

Bars in A, F, and G are the mean ± s.d. of 3 independent experiments. Statistical analysis comparing experimental to the control ('Dox-' or 'Dox- / IR-') was performed using Brown-Forsythe and Welch ANOVA followed by Dunnett's T3 multiple comparisons test (* $P \leq 0.05$; ** $P \leq 0.01$, *** $P \leq 0.001$, **** $P \leq 0.0001$, NS $P > 0.05$).

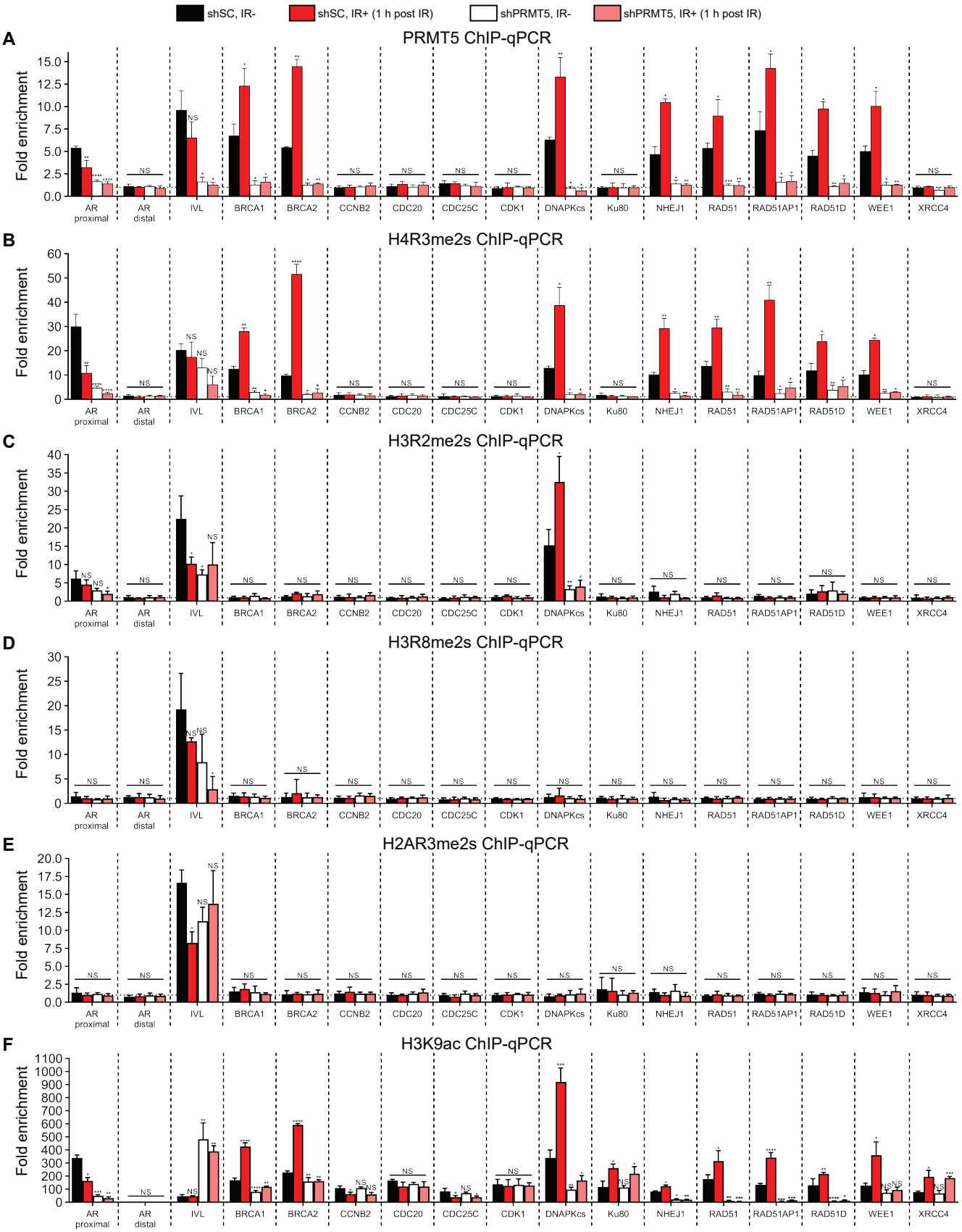

Figure S4. PRMT5 likely functions as an epigenetic activator of DDR genes. Related to figure 4.

(A)-(F) Quantification of enrichment (A: PRMT5, B: H4R3me2s, C: H3R2me2s, D: H3R8me2s, E: H2AR3me2s and F: H3K9ac) at the promoter region of the indicated genes 1 h post 2 Gy IR in irradiated (IR+) and non-irradiated (IR-) LNCaP-shSC or shPRMT5 cells via ChIP-qPCR. For each biological replicate, the value for ChIP was normalized to the value for IgG to calculate the fold enrichment (See also Figures 4C-E and G-I).

All bars are the mean ± s.d. of 3 independent experiments. Statistical analysis was performed using Brown-Forsythe and Welch ANOVA followed by Dunnett's T3 multiple comparisons test and the comparison to the control ('shSC, IR-') is shown (* $P \leq 0.05$; ** $P \leq 0.01$, *** $P \leq 0.001$, **** $P \leq 0.0001$, NS $P > 0.05$).

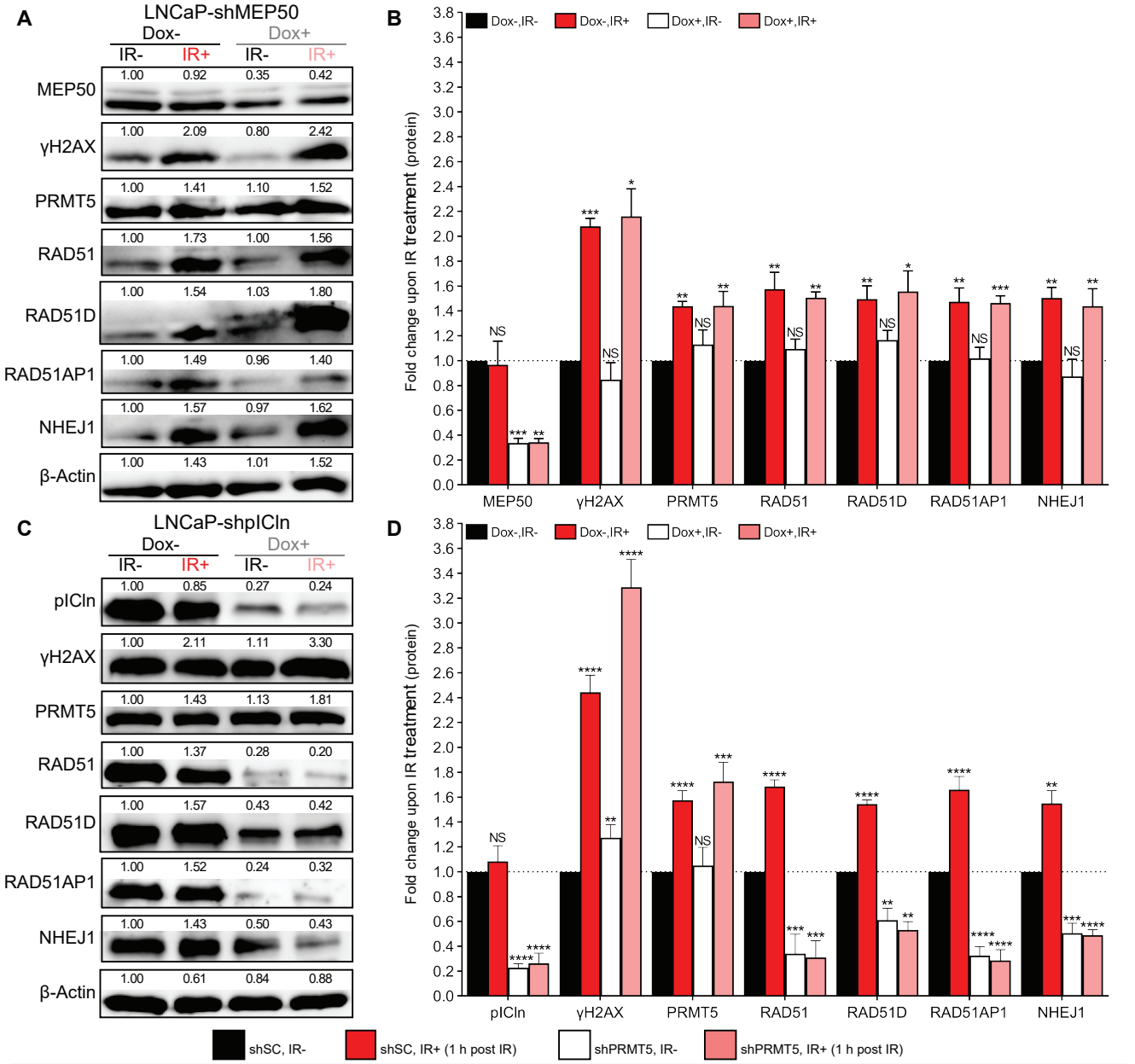
A
LNCaP-shMEP50
Dox-
Dox+
IR-
IR+
MEP50
γH2AX
PRMT5
RAD51
RAD51D
RAD51AP1
NHEJ1
β-Actin
B
Dox-,IR-
Dox-,IR+
Dox+,IR-
Dox+,IR+
Fold change upon IR treatment (protein)
C
LNCaP-shPICln
pICln
D
shSC, IR-
shSC, IR+ (1 h post IR)
shPRMT5, IR-
shPRMT5, IR+ (1 h post IR)
E
MEP50 ChIP-qPCR
Fold enrichment
IVL
BRCA1
BRCA2
CCNB2
CDC20
CDC25C
CDK1
DNAPKcs
Ku80
NHEJ1
RAD51
RAD51AP1
RAD51D
WEE1
XRCC4
F
pICln ChIP-qPCR
LNCaP, IR-
LNCaP, IR+ (1 h post IR)
G
RioK1 ChIP-qPCR
H
COPR5 ChIP-qPCR

Figure S5. pICln is also required for transcriptional activation of DDR genes and for efficient repair of DSBs. Related to Figure 5.

(A) Representative western blots showing protein expression at 2 h post 2 Gy IR in irradiated (IR+) and non-irradiated (IR-) LNCaP-shMEP50 cells with (Dox+) and without (Dox-) MEP50 knockdown. Values shown indicate the intensity relative to 'Dox-,IR-' for the biological replicate used as the representative western blot.
(B) Quantification of protein expression via western blotting from A. For each biological replicate, values were normalized to the value for 'Dox-,IR-' to calculate the fold change in protein expression upon treatment.
(C) Representative western blots showing protein expression at 2 h post 2 Gy IR in irradiated (IR+) and non-irradiated (IR-) LNCaP-shpICln cells with (Dox+) and without (Dox-) pICln knockdown. Values shown indicate the intensity relative to 'Dox-,IR-' for the biological replicate used as the representative western blot.
(D) Quantification of protein expression via western blotting from C. For each biological replicate, values were normalized to the value for 'Dox-,IR-' to calculate the fold change in protein expression upon treatment.
(E)-(F) Quantification of enrichment (E: MEP50 and F: pICln) at the promoter region of the indicated genes 1 h post 2 Gy IR in irradiated (IR+) and non-irradiated (IR-) LNCaP-shSC or shPRMT5 cells via ChIP-qPCR. Dox was applied to establish and maintain PRMT5 knockdown (shPRMT5) or express scramble control shRNA (shSC). For each biological replicate, the value for IP was normalized to the value for IgG to calculate the fold enrichment (See also Figure 5G and 5H).
(G)-(H) Quantification of enrichment (G: RioK1 and H: COPR5) at the promoter region of the indicated genes 1 h post 2 Gy IR via ChIP-qPCR in irradiated (IR+) and non-irradiated (IR-) LNCaP cells via ChIP-qPCR. For each biological replicate, the value for IP was normalized to the value for IgG to calculate the fold enrichment.

Bars in B and E-H are the mean ± s.d. of 3 independent experiments. Bars in D are the mean ± s.d. of 6 independent experiments. Statistical analysis for B, D, E, and F was performed using Brown-Forsythe and Welch ANOVA followed by Dunnett's T3 multiple comparisons test and the comparison to the control ('shSC, IR-') is shown while for G and H, statistical analysis comparing experimental to the control ('IR-') was performed using Welch's t-test (* $P \leq 0.05$; ** $P \leq 0.01$, *** $P \leq 0.001$, **** $P \leq 0.0001$, NS $P > 0.05$).

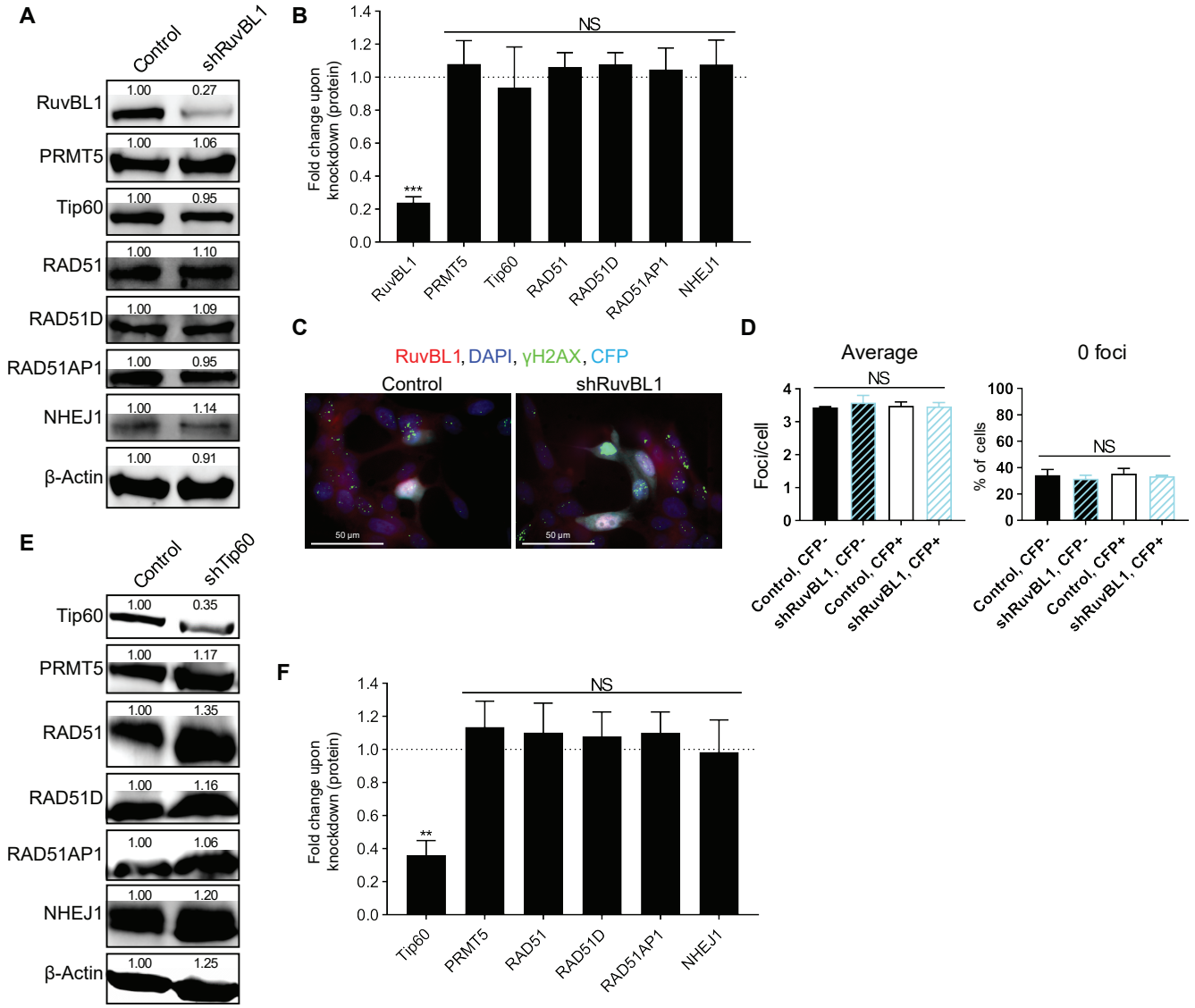

Figure S6. The transcriptional regulation of DSB repair genes by PRMT5 is not dependent on RuvBL1 or Tip60. Related to Figure 4.

(A) Representative western blot showing the protein expression in LNCaP cells with (shRuvBL1) and without (control) RuvBL1 knockdown. Values shown indicate the intensity relative to control for the biological replicate used as the representative western blot.
(B) Quantification of protein expression via western blotting from A. For each biological replicate, values were normalized to the value for 'control' to calculate the fold change in protein expression upon RuvBL1 knockdown.
(C) DSBs 6 h post 2 Gy IR in LNCaP cells with (shRuvBL1) and without (control) RuvBL1 knockdown.
(D) Quantification of DSBs in each individual cell from C as described in Figure 2B. CFP was used as a transfection control such that RuvBL1 was knocked down solely in CFP+ cells
(E) Representative western blot showing the protein expression in LNCaP cells with (shTip60) and without (control) Tip60 knockdown. Values shown indicate the intensity relative to control for the biological replicate used as the representative western blot.
(F) Quantification of protein expression via western blotting from E. For each biological replicate, values were normalized to the value for 'control' to calculate the fold change in protein expression upon Tip60 knockdown.

Fluorescence images in C are representative immunocytochemistry images (blue = DAPI, red = RuvBL1, and cerulean = CFP). Bars in B, D, and F are the mean ± s.d. of 3 independent experiments. Statistical analysis for B and F comparing experimental to the control ('control') was performed using Welch's t-test while statistical analysis for D was performed using Brown-Forsythe and Welch ANOVA followed by Dunnett's T3 multiple comparisons test (* $P \leq 0.05$; ** $P \leq 0.01$, *** $P \leq 0.001$, **** $P \leq 0.0001$, NS $P > 0.05$).

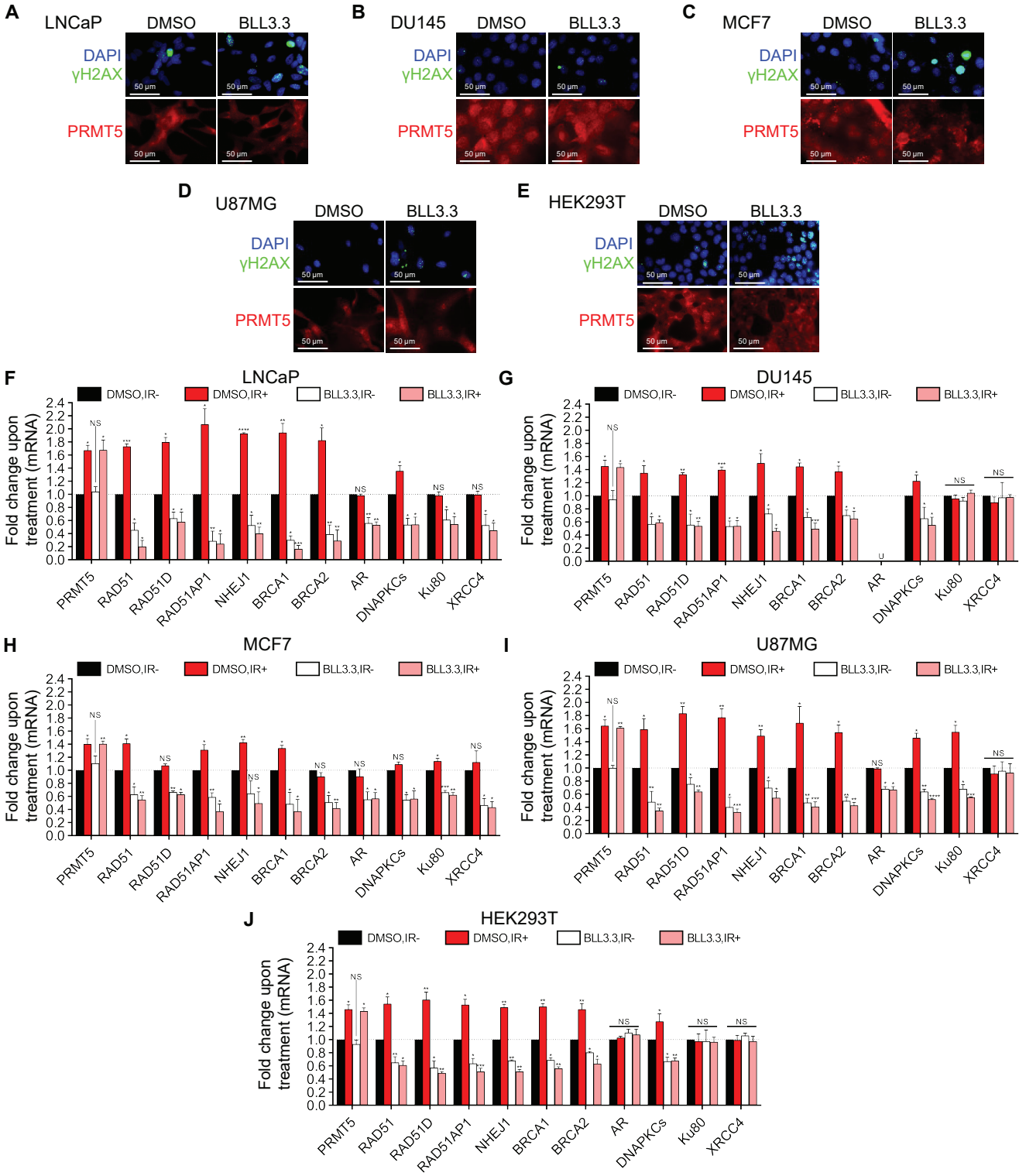

Figure S7. The role of PRMT5 in the repair of DSBs is conserved in multiple cancer cell lines. Related to Figure 7.

(A)-(E) DSBs 6 h post 2 Gy IR in the indicated cell lines (A: LNCaP, B: DU145, C: MCF7, D: U87MG, E: HEK293T) with PRMT5 inhibition (BLL3.3) or without PRMT5 inhibition (DMSO) as described in Figure 2B. Fluorescence images in A-E are representative immunocytochemistry images (blue = DAPI, green = γH2AX, and red = PRMT5) (see also Figure 7A for statistical analysis).
(F)-(J) Quantification of mRNA via RT-qPCR 6 h post 2 Gy IR in the indicated irradiated (IR+) and non-irradiated (IR-) cell lines (F: LNCaP, G: DU145, H: MCF7, I: U87MG, J: HEK293T) with PRMT5 inhibition (BLL3.3) or without PRMT5 inhibition (DMSO). For each biological replicate, values were normalized to the value for 'DMSO,IR-' (untreated) to calculate the fold change in mRNA expression upon treatment. (See also Figure 7B).

Bars are the mean ± s.d. of 3 independent experiments. Statistical analysis comparing experimental to the control ('DMSO,IR-') was performed using Brown-Forsythe and Welch ANOVA followed by Dunnett's T3 multiple comparisons test (* $P \leq 0.05$; ** $P \leq 0.01$, *** $P \leq 0.001$, **** $P \leq 0.0001$, NS $P > 0.05$).

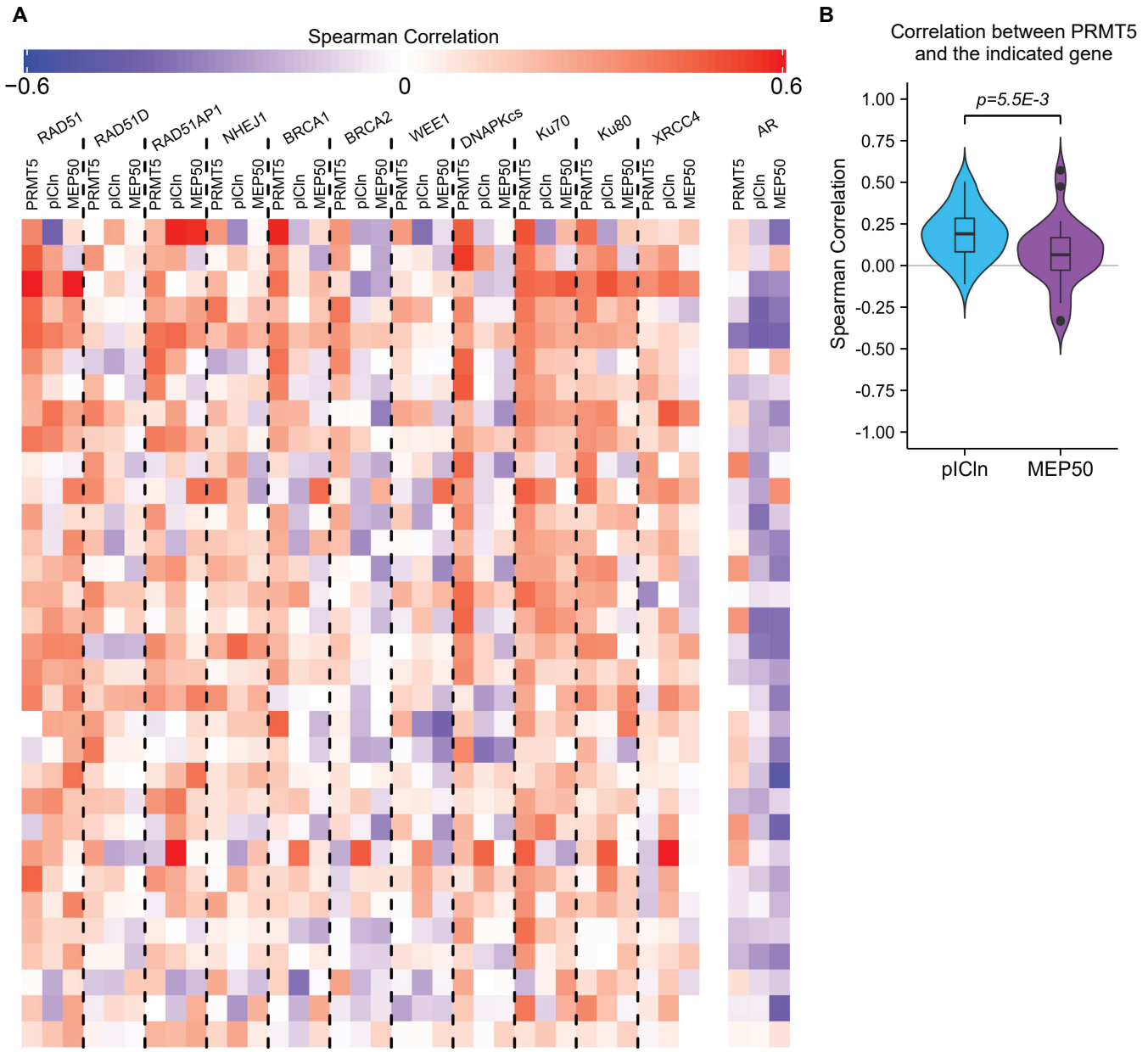

Figure S8. The expression of PRMT5 and pICln correlates with the expression of DDR genes in most human cancer tissues. Related to Figure 7.

(A) Heatmap of Spearman correlation values between the indicated DDR genes and either PRMT5, CLNS1A (pICln), or WDR77 (MEP50) at the mRNA level across 32 clinical cancer data sets. The right section shows the correlation values between AR and PRMT5, pICln, or MEP50, respectively. Red indicates a positive correlation while blue indicates a negative correlation. The cancer types (y-axis, not listed) were sorted by the mean value of correlations between PRMT5 and DDR genes. (See also Figures 7C-7E).
(B) Violin plot representation of Spearman correlation values between CLNS1A (pICln) or WDR77 (MEP50) and PRMT5.

Box-and-whiskers plots in B show the median value (line) and interquartile range between the first and third quartiles (box). The upper whisker extended to the largest value no further than '1.5 x interquartile range' and the lower whisker extended to the smallest value at most '1.5 x interquartile range'. Statistical analysis was performed using Wilcoxon test and the p-values are displayed.

LIST OF SUPPLEMENTAL FILES

Table S1 - RNA-seq in IR- cells, Related to Figure 3G
Table S2 - RNA-seq in IR+ cells, Related to Figure 3G
Table S3 - DEGs in IR+ cells, Related to Figure 3H
Table S4 - GO analysis, Related to Figure 3I
Table S5 - IPA in IR+ cells, Related to Figure 3J
Table S6 - Antibodies list, Related to Methods
Table S7 - Primers list, Related to Methods

TRANSPARENT METHODS

Cell lines and cell culture. LNCaP, DU145, PC3, and HEK293T were purchased from ATCC (Manassas, VA, USA) and cultured as described previously (Deng et al., 2017; Zhang et al., 2014). MCF7 cells were a gift from the Chun-Ju (Alice) Chang lab, and U87MG cells were a gift from the Emily Dykhuizen lab. Upon arrival, all cell lines were immediately expanded and aliquots were prepared and stored in liquid nitrogen. Cells were maintained for no longer than 30 passages or no longer than three months as described previously (Deng et al., 2011; Hsu and Hu, 2013). Cell line authentication for LNCaP cells was performed by IDEXX BioResearch (IMPACT I) and the absence of mycoplasma contamination for all cell lines was verified using LookOut® PCR Mycoplasma Detection Kit (Sigma, St. Louis, MO, USA). Knockdown cell lines were generated using the pLKO-Tet-On system. The pLKO-Tet-On plasmid for shRNA expression was obtained from Addgene (Cambridge, MA, USA) (Wiederschain et al., 2009), and shRNA sequences that target PRMT5 #1 (5'-CCCATCCTCTTCCCTATTAAG-3': referring to #1832) (Deng et al., 2017), PRMT5 #2 (5'-GCCCAGTTTGAGATGCCTTAT-3': referring to #1577) (Deng et al., 2017), SC (5'- CAACAAGATGAAGAGCACCAA-3'), MEP50 (5'- CCTCACAAGGACTCTGTGTTT-3'), and pICln (5'-CCAACAGTTGCTGGACAGTTT-3') were used for the construction of plasmids for stable cell line generation as described previously (Deng et al., 2017; Hsu and Hu, 2013). Lentiviral stably infected pools with Dox-inducible expression of PRMT5-targeting shRNA (shPRMT5 #2: referring to #1577 (Deng et al., 2017)) (LNCaP-shPRMT5 pool, PC3-shPRMT5 pool, and DU145-shRNA pool) were established and used for clonogenic assays. Stable cell lines with Dox-inducible expression of PRMT5-targeting shRNA (LNCaP-shPRMT5: referring to #1832 (Deng et al., 2017), LNCaP-shPRMT5 #2: referring to #1577 (Deng et al., 2017)) or scramble control-targeting shRNA (shSC) (LNCaP-shSC, PC3-shSC, and DU145-shSC) were established from individual clones and characterized previously (Deng et al., 2017). Stable cell lines with Dox-inducible expression of MEP50-targeting shRNA or pICln-targeting shRNA (LNCaP-shMEP50 and LNCaP-shpICln) were established from individual clones and characterized in this study.

Dox-induced knockdown and inhibitor treatment conditions. For Dox-inducible cell lines, Dox was applied at the final concentration of 1 μg/mL every 48 h to establish and maintain PRMT5 knockdown (shPRMT5), MEP50 knockdown (shMEP50), pICln knockdown (shpICln), or express scramble control shRNA (shSC). The number of days of Dox treatment was optimized: shPRMT5 and shSC cells were grown for 4 days and had 4 days of Dox treatment, shMEP50 were grown for 4 days and had 2 days of growth followed by 2 days of Dox treatment, and shpICln cells were grown for 5 days and had 5 days of Dox treatment. For parental cell lines, cells were treated with the PRMT5 inhibitor BLL3.3 (10 μM) or an equal volume of DMSO (control) every 48 h beginning 24 h after plating to inhibit PRMT5 activity. For IR experiments, cells were subjected to IR following the knockdown or inhibitor treatment described above.

Ionizing radiation conditions. For clonogenic assays, cells were irradiated using the GC-220 device (Atomic Energy of Canada, Ottawa, Canada) with a Co-60 radiation source as described previously (Deng et al., 2008, 2011). For all other experiments, cells were irradiated using the X-RAD 320 biological irradiator device (PXi Precision X-Ray, North Branford, CT, USA) with an x-ray tube radiation source at an average dose rate of ~1 Gy/25 sec. All IR treatments were carried out in normal air at room temperature, and cells spent minimal time outside incubators during treatment. Non-irradiated controls were 'mock-irradiated' by being taken out of the incubator for the same time period as irradiated counterparts.

Clonogenic assays. Clonogenic assays to quantify the surviving fraction following IR was performed similar to previously reported (Deng et al., 2008, 2011). For Dox-inducible cell lines, Dox was applied at the final concentration of 1 μg/mL every 48 h to establish and maintain PRMT5 knockdown (shPRMT5) or express scramble control shRNA (shSC). Additionally, LNCaP cells were treated with the PRMT5 inhibitor BLL3.3 (10 μM) or an equal volume of dimethyl sulfoxide (DMSO) (control) every 48 hours beginning 24 hours after plating to inhibit PRMT5 activity. After 4 days, when cells reached ~80% confluency, cells were subjected to the indicated dose of IR and immediately harvested, collected, counted, and reseeded on fresh 6 well plates for clonogenic assay. After 14 days of growth, the number of colonies were counted to calculate the surviving fraction. The number of cells for reseeding was optimized based upon how much cell death was observed: (LNCaP: 0 Gy-500 cells, 2 Gy-700 cells, 4 Gy-1000 cells, 6 Gy-5000 cells, and 8 Gy-10000 cells), (PC3: 0 Gy-50 cells, 2 Gy-100 cells, 4 Gy-200 cells, 6 Gy-600 cells, and 8 Gy-1000 cells), (DU145: 0 Gy-50 cells, 2 Gy-100 cells, 4 Gy-200 cells, 6 Gy-400 cells, and 8 Gy-800 cells).

Immunocytochemistry (ICC) for quantification of IR-induced DSBs (Kuo and Yang, 2008)**, NHEJ-associated foci** (Rapp, 2004; Slupianek et al., 2006)**, and HR-associated foci** (Rapp, 2004; Slupianek et al., 2006). Cells were seeded on 6 cm dishes containing glass coverslips and treated as described elsewhere. When cells reached ~80% confluency, cells were treated with 2 Gy IR and then fixed with 3.7% formaldehyde in phosphate buffered saline (PBS) at room temperature for 20 minutes at the indicated time points: First, we assessed the formation and repair of DSBs by analyzing γH2AX foci in a time course following radiation (5 m and 1, 2, 6, and 24 h). Given that the majority of DSBs are repaired within 2-6 h following IR, we assessed the effect of knockdown or inhibitor on the repair of DSBs at the 6 and 24 h timepoints. To assess potential impact on HR or NHEJ, we assessed RAD51 and Ku70 foci, respectively, at 1 h following IR treatment which is when the majority of repair occurred. After fixation at the indicated timepoints, cells were permeabilized with 0.2% Triton X-100 in PBS at room temperature for 5 m. Cells were then blocked with 5% milk blocking solution in PBS, stained with the indicated primary antibodies diluted in 5% milk blocking solution in PBS, and stained with 4,6-diamidino-2-phenylindole (DAPI final 10 µg/mL) and indicated secondary antibodies diluted in 5% milk blocking solution in PBS. Cells on coverslips were mounted on glass slides using the ProLong® Antifade Kit (Invitrogen Molecular Probes, Eugene, OR, USA) and sealed with clear nail polish. Cells were then imaged via the Nikon TE2000 inverted fluorescence microscope under oil immersion (60x objective) (Nikon Instruments Melville, NY, USA). The number of foci was manually recorded for each cell (defined via nuclear DAPI staining). At least 60 cells were counted for each biological replicate. The arrays of foci counts for each biological replicate were subjected to further analysis separately to determine the average number of foci per cell and percentage of cells with zero foci. The primary antibodies used were anti-PRMT5-rabbit (1:1000), -γH2AX-mouse (1:1000), -γH2AX-rabbit (1:200), -AR-mouse (1:1000), -AR-rabbit (1:100), -RAD51-rabbit (1:1000), -Ku70-mouse (1:500), -MEP50-rabbit (1:100), -pICln-rabbit (1:1000), and -RuvBL1-rabbit (1:100). Secondary antibodies used were anti-mouse-FITC (1:100) and anti-rabbit-rhodamine red (1:1000). All antibodies are described in **Table S6**.

Immunocytochemistry (ICC) for quantification of protein expression or subcellular localization. Immunocytochemistry was performed as described above. Images were analyzed via ImageJ (Schneider et al., 2012). First, the background was subtracted from the image using the rolling ball method (http://imagej.net/plugins/rolling-ball.html). For PRMT5 expression, regions of interest (ROI) were outlined for each individual cell. For AR expression, ROI were outlined for each nucleus (as defined by DAPI staining). For MEP50 and pICln expression and subcellular localization, ROI were outlined for each individual cell, nucleus only (as defined by DAPI staining), and cytoplasm only (as defined by signal outside of DAPI staining). The average intensity for each ROI was measured and at least 60 cells were counted for each biological replicate. The arrays of intensity counts for each biological replicate were subjected to further analysis separately and were analyzed via both “D’Agostino & Pearson” and “Shapiro-Wilk” normality tests to evaluate distribution. Because not all samples were normally distributed, the median value was used for each biological replicate. To determine the nuclear:cytoplasmic ratio (N:C) the value for nucleus was divided by the value for cytoplasmic for each cell individually such that an N:C ratio of 1 indicates equal expression in both the nucleus and cytoplasm.

Comet assay. To determine if PRMT5 regulates the repair of IR-induced DSBs, we used comet assay to quantify DNA damage directly. LNCaP-shPRMT5 cells were seeded on 6 cm dishes and Dox was applied at the final concentration of 1 µg/mL every 48 h to establish and maintain PRMT5 knockdown. After 4 days, when cells reached ~80% confluency, cells were treated with the indicated dose of IR and then harvested and counted after either 5 m or 2 h. The 5 m timepoint indicates how much total DNA damage is induced by radiation. Comparing the 2 h timepoint to the 5 m timepoint indicates how much DNA damage is repaired. Twenty thousand cells per group were diluted in 100 µL of 0.5% Low Melting Agarose in PBS at 45°C and 50 µL of diluted cells were immobilized onto pretreated VWR Superfrost Plus slides (previously dipped in 1% Agarose in nanopure water and allowed to dry overnight). Glass coverslips were placed on top of the cell dilution and the slides were placed in 4°C for 10 minutes to solidify the agarose. Slides were moved to room temperature for 5 minutes, the coverslips removed, and immobilized cells were lysed in 4°C neutral lysis buffer (10mM Tris HCl pH 8.0, 100 mM EDTA, 2.5 M NaCl, 1% Sarkosyl, 0.5% Triton X-100) for 60 minutes at 4°C. Slides were removed from lysis buffer and equilibrated in Neutral Comet Electrophoresis Buffer (90 mM Tris HCl pH 8.0, 90 mM Boric Acid, 2 mM EDTA) for 20 minutes. Electrophoresis was performed at 14V, 27mA for 60 minutes. After electrophoresis, slides were equilibrated in 0.4 M Tris-HCl pH 7.4 for 5 minutes at room temperature. The equilibration buffer was replaced with fresh buffer, and the slides were incubated for an additional 5 minutes. This wash was repeated one additional time for a total of three washes. Sixty µL of DAPI (0.5 µg/mL in H_2O) was applied dropwise to the agarose pad, and slides were incubated at 4°C for 15 minutes. Comets were then imaged via the Nikon TE2000 inverted fluorescence microscope (20x objective) (Nikon Instruments Melville, NY, USA) and analyzed with ImageJ (Schneider et al., 2012). To quantify the ‘% tail DNA’ in each cell from the images, we utilized the comet assay plugin created by Robert Bagnell (2011) based on the NIH Image comet assay by Herbert M. Miller (1997). At least 65 cells were analyzed across 3 biological replicates and the ‘% tail DNA’ values were pooled for statistical analysis via Mann-Whitney *U*-test. Although several reports using comet assay have used various data representation and statistical analysis (Higo et al., 2017; Lee et al., 2017; Mo et al., 2018; Nassour et al., 2016), because of the high variance within each biological replicate and lack of normal distribution we used the Mann-Whitney *U*-test (Dungrawala et al., 2017; Liu et al., 2018; Xiao et al., 2018).

Etoposide treatment. To assess if PRMT5 is required for repair of DSBs in general, we used etoposide to induce replication-dependent DSBs. LNCaP-shPRMT5 cells were seeded on 6 cm dishes containing glass coverslips and Dox was applied at the final concentration of 1 µg/mL every 48 h to establish and maintain PRMT5 knockdown. When cells reached ~60% confluency, cells were treated with either etoposide (10 µM) or an equal volume of DMSO. Forty-eight h after initiation of treatment, coverslips were transferred to a new dish and subjected to γH2AX-foci analysis described above while the remaining cells were harvested and subjected to western blot analysis. Although not shown, experiments with short etoposide treatments (2 h, 6 h) were unsuccessful and the 48 h etoposide treatment time was likely optimal because cells could undergo DNA replication which induced DSBs.

Transient transfection for rescue of AR expression. To evaluate if the role of PRMT5 in the repair of IR-induced DSBs is independent of AR, LNCaP-shPRMT5 cells were seeded on 6 cm dishes containing glass coverslips and Dox was applied at the final concentration of 1 µg/mL every 48 h to establish and maintain PRMT5 knockdown. Forty-eight h following seeding, cells were transfected with pCMV-Flag2-AR, as described previously (Deng et al., 2017; Hsu and Hu, 2013), or pCMV-Empty Vector plasmid using FuGENE HD (Promega, Madison, Wisconsin, USA). pCMV-HA-CFP was used as a transfection control. Upon reaching ~80% confluency (48 h following transfection), cells were treated with 2 Gy IR and subjected to immunocytochemistry analysis. Only transfected cells (CFP+) were subjected to γH2AX foci analysis, while both transfected and non-transfected cells were subjected to protein expression analysis as described above. For the microscope images, we used 3D representation to show the expression of multiple proteins in a single cell at the same time. Each peak is a cell and the height of each peak is the intensity of signal.

RNA-seq for identification of PRMT5 target genes in response to IR. LNCaP-shPRMT5 cells were seeded on 6 cm dishes and Dox was applied at the final concentration of 1 µg/mL every 48 h to establish and maintain PRMT5 knockdown for 4 days. Cells were harvested 1 h following a 2 Gy IR treatment and total RNA was isolated using Trizol Reagent (Ambion, Carlsbad, CA, USA). PolyA+ RNA libraries were generated according to the Illumina "TruSeq Stranded mRNA Sample Preparation Guide" (15031047E) with the following considerations: (1) an Agilent Bioanalyzer RNA-Nano kit was used to assess RNA concentration and rule out sample degradation. (2) Heat and divalent cation fragmentation of the polyA+ RNA was undertaken for 4 m rather than the default of 8 m. (3) The number of PCR cycles for library amplification was determined by the yield of cDNA. For both RNA-seq analyses, we ran 8 cycles of PCR instead of the 15 cycles mentioned in the manual. (4) Final cleanup was performed using a 0.8:1 bead:sample ratio with AmPure XP beads instead of the 1:1 mentioned in the manual. IR+ group was run on an Illumina HiSeq 2500 using High Output flowcell to produce paired-end 101 base reads. IR- group was run on an Illumina NovaSeq 6000 S4 flowcell that generated paired-end 151 base reads. Additionally, IR- samples were prepared and run with unique dual indexes to mitigate potential "index-hopping" associated with Illumina instruments using "exclusion amplification" clustering on patterned flowcells.

RNA-seq quality was assessed by FastQC, and STAR RNA-seq aligner (Dobin et al., 2013) was used to map all high-quality sequences to the human genome (GENCODE GRCh38). Read counts were evaluated using Subread featureCounts (Liao et al., 2014) to summarize uniquely mapped reads to the gene level according to the GENCODE M25 annotation file. Data was normalized by trimmed mean of M value method to obtain the final profile of gene expression (base-2 log scale). EdgeR (Robinson et al., 2010) was used to perform differential expression analysis by comparing Dox+ (PRMT5 KD) and Dox- (no KD) for IR+ and IR- groups. After removing low-expressed genes (average expression levels lower than 1 for both conditions), we defined genes as differentially expressed genes (DEGs) if their FDR-adjusted p-values were less than 0.01, and the magnitudes of fold-changes (FCs) were larger than log2 (1.25).

Gene Ontology (GO) and pathway analysis were performed on the 'IR+ only' DEGs. GO analysis was performed using the web-based tool DAVID functional annotation analysis (http://david.abcc.ncifcrf.gov/home.jsp v6.8) (Huang et al., 2007, 2009). Only GO annotations with FDR-adjusted p-values less than 0.05 and the fold enrichment score larger than 1.5 were selected as significantly over-represented GO terms. Pathway analysis on IR+ only DEGs was performed using Ingenuity Pathway Analysis (IPA) (QIAGEN Inc., https://www.qiagenbioinformatics.com/products/ingenuity-pathway-analysis) to identify differentially regulated pathways upon PRMT5 knockdown in irradiated cells.

RNA isolation, reverse transcription, and RT-qPCR. Cells were seeded on either 6 cm or 10 cm dishes and treated as described elsewhere. Total RNA was isolated using Trizol Reagent (Ambion, Carlsbad, CA, USA). RNA concentration and integrity were verified by agarose gel electrophoresis. cDNA synthesis was done using High Capacity cDNA Reverse Transcription Kit (Promega, Madison, WI, USA) as described previously (Deng et al., 2017; Hsu and Hu, 2013; Zhang et al., 2014). qPCR was performed using FastStart Universal SYBR Green Master Mix (Thermo Fisher Scientific, Waltham, MA, USA) on the QuantStudio 6 Flex System and QuantStudio™ Real-Time PCR Software (ThermoFisher, Waltham, MA, USA). Forty cycles were run and samples without C_T values were deemed undetected. Technical duplicates were run for each sample and the C_T values used for further analysis were the average of the technical duplicates. Samples where C_T values for technical duplicates were >0.5 apart were re-run. Non-template controls (NTC)s with autoclaved double-distilled H_2O were also run for each primer set and primer sets where C_T values for NTC were lower than 37 (indicating high background) were re-run. Amplicon size and specificity were verified for each primer set via agarose gel electrophoresis. PRMT5, AR, and GAPDH primers were used previously (Deng et al., 2017; Zhang et al., 2014). IVL primers were used previously (Chew et al., 2013; Saha et al., 2016). All primers used are described in **Table S7**.

Chromatin immunoprecipitation (ChIP)-qPCR assay. LNCaP-shPRMT5 or LNCaP-shSC cells were seeded on multiple 10 cm dishes and Dox was applied at the final concentration of 1 µg/mL every 48 h to establish and maintain PRMT5 knockdown (shPRMT5) or express scramble control shRNA (shSC). After 4 days, when cells reached ~80% confluency, cells were treated with 2 Gy IR. One hour following IR (prior to the repair of the majority of DSBs and at the same time as the peak of IR-induced PRMT5 protein expression), cells were fixed/crosslinked and chromatin was prepared for ChIP-qPCR as described previously (Deng et al., 2017). Chromatin fragments were verified to be ~500 base pairs by agarose gel electrophoresis. Antibodies used for immunoprecipitation were anti-PRMT5-rabbit, -H4R3me2s-rabbit, -H3K9ac-rabbit, -H3R2me2s-rabbit, -H3R8me2s-rabbit, -H2AR3me2s-rabbit, -MEP50-rabbit, -pICln-rabbit, and IgG-rabbit. All antibodies are described in **Table S6**. Primers used for ChIP-qPCR are described in **Table S7**.

Flow cytometry cell-cycle analysis. LNCaP-shPRMT5 cells were seeded on 6 cm dishes and Dox was applied at the final concentration of 1 µg/mL every 48 h to establish and maintain PRMT5 knockdown. After 4 days, when cells reached ~80% confluency, IR+ cells were treated with 2 Gy IR. Cells were harvested 24 h following IR, resuspended in PBS, and filtered through a 70 µm nylon cell strainer to remove all cell aggregates. A single cell suspension was prepared and verified via microscopy. Cells were then fixed in 70% ethanol, stained with a Propidium Iodide (PI) containing solution (20 µg/mL PI and RNaseA diluted in PBS) and subjected to flow cytometry analysis via the Guava EasyCyte Flow Cytometer (Guava Technologies, Hayward, CA, USA). At least 20,000 live cells were counted for each biological replicate. Flow cytometry data was analyzed via FlowJo (FlowJo, LLC, Ashland, Oregon, USA). Live cells were gated for analysis to remove any sub-G_1 cells and then were subjected to cell cycle analysis via Dean-Jett-Fox modeling (Fox, 1980).

Western blot. Cells were seeded on either 6 cm or 10 cm dishes and treated as described elsewhere. Cells were harvested in lysis buffer (100 mM Tris-HCl pH 8.0, 15 mM $MgCl_2$, 100 mM KCl, 5 µg/mL of each Chymostatin, Leupeptin, Pepstatin A, and antipan in DMSO, 1% Triton X-100, 1 mM PMSF in ethanol, and 1 mM DTT) or RIPA buffer (10 mM Tris-HCl pH 8.0, 5 mM EDTA, 1% Triton X-100, 0.1% Sodium Deoxycholate, 0.1% SDS, 140 mM NaCl, 5 µg/mL of each Chymostatin, Leupeptin, Pepstatin A, and antipan in DMSO, and 1 mM PMSF in ethanol) and total protein concentration was measured using Bradford method. Approximately 20-30 µg total protein was run on a 10-15% SDS-PAGE and western blotting was performed as described previously (Deng et al., 2017; Hsu and Hu, 2013; Zhang et al., 2014). Band/protein intensity was quantified using Image Lab™ (Bio-rad, Hercules, CA, USA). Antibodies used for western blot were anti-PRMT5-rabbit (1:1000), -AR-rabbit (1:2000), -γH2AX-rabbit (1:1000), -RAD51-rabbit (1:2000), -RAD51D-rabbit (1:2000), -RAD51AP1-rabbit (1:1000), -NHEJ1-rabbit (1:2000), -β-Actin-mouse (1:2000), -MEP50-rabbit (1:500), -pICln-rabbit (1:2000), -RuvBL1-rabbit (1:1000), -Tip60-rabbit (1:500), -rabbit-HRP (horseradish peroxidase) (1:1000), -mouse-HRP (1:1000). All antibodies are described in **Table S6**.

Bimolecular Fluorescence Complementation (BiFC) assay. LNCaP cells were grown to ~60% confluency and transfected with plasmids to visualize the PRMT5:MEP50 interaction (pMYC-VN155-PRMT5, pHA-VC-MEP50, and pFlag-NLS-CFP) and PRMT5:pICln interaction (pMYC-VN155-PRMT5, pHA-VC-pICln, and pFlag-NLS-CFP). Forty-eight hours following transfection, cells were treated with 2 Gy IR. Immediately prior to IR and 6 h following IR (the time point with the largest changes in MEP50 and pICln subcellular localization), cells were imaged via the Nikon TE2000 inverted fluorescence microscope (20x objective) (Nikon Instruments Melville, NY, USA). Images were then analyzed with ImageJ (Schneider et al., 2012). First, the background was subtracted from the image using the rolling ball method (http://imagej.net/plugins/rolling-ball.html). ROI were outlined for each individual cell, nucleus only (as defined by NLS-CFP staining), and cytoplasm only (as defined by staining outside NLS-CFP signal). The average intensity for each ROI was measured and at least 50 cells were counted for each biological replicate. The arrays of intensity counts for each biological replicate were subjected to further analysis separately and were analyzed via both “D’Agostino & Pearson” and “Shapiro-Wilk” normality tests to evaluate distribution. Because not all samples were normally distributed, the median value was used for each biological replicate. To determine the nuclear:cytoplasmic ratio (N:C) the value for nucleus was divided by the value for cytoplasmic for each cell individually such that an N:C ratio of 1 indicates equal protein-protein interaction in both the nucleus and cytoplasm.

Transient knockdown of RuvBL1 and Tip60. To confirm that the mechanism we describe here is independent of PRMT5-mediated regulation of RuvBL1 and Tip60, we performed similar assays with knockdown of RuvBL1 or Tip60. First, we obtained MISSION® shRNA bacterial glycerol stocks containing shRNA expression plasmids (RuvBL1: TRCN0000018911, TRCN0000018912, TRCN0000018913, TRCN0000018914, and TRCN0000319216. Tip60: TRCN0000020314, TRCN0000020315, TRCN0000020317, TRCN0000020318, and TRCN0000298504) (Sigma-Aldrich/Millipore Sigma, St. Louis, Missouri, USA). Using maxiprep, we isolated the shRNA expression plasmids and generated viral particles in HEK293T cells as described previously (Hsu and Hu, 2013) via co-transfection of all 5 shRuvBL1 or all 5 shTip60 expression plasmids along with pCMV-HA-CFP as a control. Although we could have used transient transfection of individual shRNA expression plasmids, we used viral particle transduction with all 5 shRNA expression vectors at once to ensure sufficient knockdown. FuGENE HD (Promega, Madison, Wisconsin, USA) was used as the transfection reagent, pHR'-CMV-8.2ΔVPR was used as the packaging plasmid, and pHR'-CMV-VSV-G was used as the envelope plasmid. Forty-eight hours following transfection, media from the HEK293T cells was collected, passed through a 0.45 µm filter, and applied to the LNCaP cells for viral particle transduction. Viral particles were applied to the LNCaP cells both 24 hours and 72 hours after plating.

LNCaP cells were transduced with either shRuvBL1 or shTip60 viral particles once and again after 48 h to establish RuvBL1 or Tip60 knockdown. Cells were then treated with 2 Gy IR and subjected to γH2AX-foci analysis and western blot analysis described above.

Correlation analysis of TCGA clinical cancer data sets. Gene expression profiles of 32 clinical cancer data sets from TCGA Pan-Cancer analysis (The Cancer Genome Atlas Research Network et al., 2013) were retrieved from cBioPortal (Cerami et al., 2012; Gao et al., 2013). Using the mRNA expression of PRMT5, pICln, MEP50, AR, and DDR genes which are primary target genes of both PRMT5 and AR, we calculated the Spearman correlations between gene pairs for each cancer type. The gene set for DDR genes was defined as RAD51, RAD51D, RAD51AP1, NHEJ1, BRCA1, BRCA2, WEE1, DNAPKcs, Ku70, Ku80, an XRCC4. Although we did not perform additional studies on Ku70, Ku70 was included as it is another well-studied, key regulator of NHEJ. In **Figure 7D**, a cutoff of $p < 0.01$ was used to determine the significance of correlation between PRMT5 and AR as either positive, negative, or no correlation if $p > 0.01$, in order to stratify the cancers into the different types.

Statistical analysis. No statistical methods were used to predetermine sample size. For the correlation analysis of TCGA clinical cancer data sets, statistical analysis was performed using Wilcoxon rank sum test in R 3.5.3. (R Core Team (2013). R: A language and environment for statistical computing. R Foundation for Statistical Computing, Vienna, Austria, https://www.R-project.org/). All other statistical analyses were performed using Graphpad Prism 7.00 and 8.00 for Windows (GraphPad Software, La Jolla California USA, www.graphpad.com). Statistical analysis for comet assay and RNA-seq analysis are described above. For all other experiments, statistical analysis was performed on raw data with assumed normal distribution. For all qPCR experiments, statistical analysis was performed on ΔC_T values (C_T value of gene normalized to C_T value of GAPDH control). For all ChIP-qPCR experiments, statistical analysis was performed on ΔC_T values (C_T value of gene normalized to C_T value of IgG control). For all western blot experiments, statistical analysis was performed on normalized raw intensity values (intensity value of protein divided by the intensity value of β-Actin). When comparing two sample groups, we used unpaired, two-tailed *t*-tests with Welch's correction (Welch's *t*-test) because standard deviations were not always equal for all groups. When comparing multiple sample groups, in order to compare the means or medians among all the samples and incorporate the standard deviation of each of the samples, Brown-Forsythe and Welch ANOVA followed by Dunnett's T3 multiple comparisons test was used. For **Figures 1A**, **1B**, **1D**, and **1E**, as the variance in the mean among samples were small and the dose-response occurred on a log scale, statistical analysis was performed using Welch's *t*-test of log-transformed data. All relevant statistics are reported in the corresponding legends.

SUPPLEMENTAL REFERENCES

Cerami, E., Gao, J., Dogrusoz, U., Gross, B.E., Sumer, S.O., Aksoy, B.A., Jacobsen, A., Byrne, C.J., Heuer, M.L., Larsson, E., et al. (2012). The cBio Cancer Genomics Portal: An Open Platform for Exploring Multidimensional Cancer Genomics Data. Cancer Discov. *2*, 401–404.

Chew, Y.C., Adhikary, G., Xu, W., Wilson, G.M., and Eckert, R.L. (2013). Protein Kinase C δ Increases Kruppel-like Factor 4 Protein, which Drives Involucrin Gene Transcription in Differentiating Keratinocytes. J. Biol. Chem. *288*, 17759–17768.

Deng, X., Liu, H., Huang, J., Cheng, L., Keller, E.T., Parsons, S.J., and Hu, C.-D. (2008). Ionizing Radiation Induces Prostate Cancer Neuroendocrine Differentiation through Interplay of CREB and ATF2: Implications for Disease Progression. Cancer Res. *68*, 9663–9670.

Deng, X., Elzey, B.D., Poulson, J.M., Morrison, W.B., Ko, S.-C., Hahn, N.M., Ratliff, T.L., and Hu, C.-D. (2011). Ionizing radiation induces neuroendocrine differentiation of prostate cancer cells in vitro, in vivo and in prostate cancer patients. Am J Cancer Res *1*, 834–844.

Deng, X., Shao, G., Zhang, H.T., Li, C., Zhang, D., Cheng, L., Elzey, B.D., Pili, R., Ratliff, T.L., Huang, J., et al. (2017). Protein arginine methyltransferase 5 functions as an epigenetic activator of the androgen receptor to promote prostate cancer cell growth. Oncogene *36*, 1223–1231.

Dobin, A., Davis, C.A., Schlesinger, F., Drenkow, J., Zaleski, C., Jha, S., Batut, P., Chaisson, M., and Gingeras, T.R. (2013). STAR: ultrafast universal RNA-seq aligner. Bioinformatics *29*, 15–21.

Dungrawala, H., Bhat, K.P., Le Meur, R., Chazin, W.J., Ding, X., Sharan, S.K., Wessel, S.R., Sathe, A.A., Zhao, R., and Cortez, D. (2017). RADX Promotes Genome Stability and Modulates Chemosensitivity by Regulating RAD51 at Replication Forks. Mol. Cell *67*, 374-386.e5.

Fox, M.H. (1980). A model for the computer analysis of synchronous DNA distributions obtained by flow cytometry. Cytometry A *1*, 71–77.

Gao, J., Aksoy, B.A., Dogrusoz, U., Dresdner, G., Gross, B., Sumer, S.O., Sun, Y., Jacobsen, A., Sinha, R., Larsson, E., et al. (2013). Integrative analysis of complex cancer genomics and clinical profiles using the cBioPortal. Sci. Signal. *6*, 1–34.

Higo, T., Naito, A.T., Sumida, T., Shibamoto, M., Okada, K., Nomura, S., Nakagawa, A., Yamaguchi, T., Sakai, T., Hashimoto, A., et al. (2017). DNA single-strand break-induced DNA damage response causes heart failure. Nat. Commun. *8*, 15104.

Hsu, C.-C., and Hu, C.-D. (2013). Transcriptional activity of c-Jun is critical for the suppression of AR function. Mol. Cell. Endocrinol. *372*, 12–22.

Huang, D.W., Sherman, B.T., Tan, Q., Collins, J.R., Alvord, W.G., Roayaei, J., Stephens, R., Baseler, M.W., Lane, H.C., and Lempicki, R.A. (2007). The DAVID Gene Functional Classification Tool: a novel biological module-centric algorithm to functionally analyze large gene lists. Genome Biol. *8*, R183.

Huang, D.W., Sherman, B.T., and Lempicki, R.A. (2009). Systematic and integrative analysis of large gene lists using DAVID bioinformatics resources. Nat. Protoc. *4*, 44–57.

Kuo, L.J., and Yang, L.-X. (2008). γ-H2AX-a novel biomarker for DNA double-strand breaks. In Vivo *22*, 305–309.

Lee, J.-H., Park, S.-J., Hariharasudhan, G., Kim, M.-J., Jung, S.M., Jeong, S.-Y., Chang, I.-Y., Kim, C., Kim, E., Yu, J., et al. (2017). ID3 regulates the MDC1-mediated DNA damage response in order to maintain genome stability. Nat. Commun. *8*, 903.

Liao, Y., Smyth, G.K., and Shi, W. (2014). featureCounts: an efficient general purpose program for assigning sequence reads to genomic features. Bioinformatics *30*, 923–930.

Liu, H., Zhang, H., Wu, X., Ma, D., Wu, J., Wang, L., Jiang, Y., Fei, Y., Zhu, C., Tan, R., et al. (2018). Nuclear cGAS suppresses DNA repair and promotes tumorigenesis. Nature *563*, 131–136.

Mo, L.-J., Song, M., Huang, Q.-H., Guan, H., Liu, X.-D., Xie, D.-F., Huang, B., Huang, R.-X., and Zhou, P.-K. (2018). Exosome-packaged miR-1246 contributes to bystander DNA damage by targeting LIG4. Br. J. Cancer *119*, 492–502.

Nassour, J., Martien, S., Martin, N., Deruy, E., Tomellini, E., Malaquin, N., Bouali, F., Sabatier, L., Wernert, N., Pinte, S., et al. (2016). Defective DNA single-strand break repair is responsible for senescence and neoplastic escape of epithelial cells. Nat. Commun. *7*, 10399.

Rapp, A. (2004). After double-strand break induction by UV-A, homologous recombination and nonhomologous end joining cooperate at the same DSB if both systems are available. J. Cell Sci. *117*, 4935–4945.

Robinson, M.D., McCarthy, D.J., and Smyth, G.K. (2010). edgeR: a Bioconductor package for differential expression analysis of digital gene expression data. Bioinformatics *26*, 139–140.

Saha, K., Adhikary, G., and Eckert, R.L. (2016). MEP50/PRMT5 Reduces Gene Expression by Histone Arginine Methylation and this Is Reversed by PKCδ/p38δ Signaling. J. Invest. Dermatol. *136*, 214–224.

Schneider, C.A., Rasband, W.S., Eliceiri, K.W., and others (2012). NIH Image to ImageJ: 25 years of image analysis. Nat Methods *9*, 671–675.

Slupianek, A., Nowicki, M.O., Koptyra, M., and Skorski, T. (2006). BCR/ABL modifies the kinetics and fidelity of DNA double-strand breaks repair in hematopoietic cells. DNA Repair *5*, 243–250.

The Cancer Genome Atlas Research Network, Weinstein, J.N., Collisson, E.A., Mills, G.B., Shaw, K.R.M., Ozenberger, B.A., Ellrott, K., Shmulevich, I., Sander, C., and Stuart, J.M. (2013). The Cancer Genome Atlas Pan-Cancer analysis project. Nat. Genet. *45*, 1113–1120.

Wiederschain, D., Susan, W., Chen, L., Loo, A., Yang, G., Huang, A., Chen, Y., Caponigro, G., Yao, Y., Lengauer, C., et al. (2009). Single-vector inducible lentiviral RNAi system for oncology target validation. Cell Cycle *8*, 498–504.

Xiao, X., Liang, J., Huang, C., Li, K., Xing, F., Zhu, W., Lin, Z., Xu, W., Wu, G., Zhang, J., et al. (2018). DNA-PK inhibition synergizes with oncolytic virus M1 by inhibiting antiviral response and potentiating DNA damage. Nat. Commun. *9*.

Zhang, H.-T., Zhang, D., Zha, Z.-G., and Hu, C.-D. (2014). Transcriptional activation of PRMT5 by NF-Y is required for cell growth and negatively regulated by the PKC/c-Fos signaling in prostate cancer cells. Biochim. Biophys. Acta BBA - Gene Regul. Mech. *1839*, 1330–1340.